Estimating forces in mixed eccentricities motion from purely dynamic eccentric rotor centre motion in a hydropower generator and their validation against EM simulations

Y. Calleecharan, R. Jauregui, and J.-O. Aidanpää

Abstract—Electromagnetic analysis of hydropower generators is common practice but there is little emphasis on studying the effect of rotor whirling in the analysis. This paper demonstrates the use of the unbalanced magnetic pull (UMP) curves based on purely dynamic eccentricity motion for a wide range of whirling frequencies in the prediction of the steady state UMP in the case of mixed eccentricities motion. The latter motion type is more realistic in practice. Actual electromagnetic (EM) simulations are also carried out for these mixed eccentricities motion cases in order to verify the proposed method. Good agreement between the UMP from the actual EM simulations and the UMP predictions are made when low eccentricities exist. The proposed method is thus very useful since firstly, very few EM software packages can handle mixed eccentricities motion and secondly, since actual EM simulations of intricate rotor centre motion are time-consuming, the proposed method is a big time saver. A modified feature selective validation (FSV) method, the FSV-UPC, is also applied to assess the similarities and the differences in the force computations.

Index Terms—eccentricity, electromagnetic simulations, hydropower, rotor, whirl

Nomenclature

γ	slot angle pitch
Γ	domain boundary
μ	magnetic permeability [H/m]
ρ	charge density [C/m^3]
σ	electrical conductivity [S/m]
ω	angular velocity [rad/s]
Ω	domain
∇	differential operator
A	magnetic vector potential [T m]
ADM	amplitude difference measure
B	magnetic flux density [T]
D	electric flux density [C/m^2]
E	electric field strength [V/m]
F	Force [N]
FDM	feature difference measure
FSV	feature selective validation
H	magnetic field strength [A/m]
J	current density [A/m^2]
t	time [s]
ODM	offset difference measure
UMP	unbalanced magnetic pull
v	velocity [m /s]

Y. Calleecharan is with the Department of Mechanical and Production Engineering, University of Mauritius, Réduit, Mauritius (email: y.calleecharan@uom.ac.mu).

R. Jauregui is with Roche Diagnostics, Barcelona, Spain (email: ricardojtpmp@gmail.com).

J.-O. Aidanpää is with the Department of Engineering Sciences and Mathematics, Luleå Tekniska Universitet, Luleå, Sweden (email: joa@ltu.se).

x	Cartesian horizontal coordinate for rotor centre
y	Cartesian vertical coordinate for rotor centre

subscripts & superscripts

c	conducting
d	dynamic
m	mixed
nc	non-conducting
ro	rotor
s	static
wh	whirl
whr	whirl ratio
0	impressed current
$pred$	predicted

I. Introduction

ROTOR-stator eccentricity in electrical machines is an issue that has caught attention for a long time [1], [2] and is an important item in condition monitoring [3] in electrical machines. Though many papers in the literature [4]–[8] have addressed the issue of eccentricity in rotating electrical machines, and other papers [9]–[12] have dealt with mixed eccentricities (where both static and dynamic eccentricities occur) motion, there has been generally a lack of papers that account for the effect of whirling of the rotor. Two publications that have considered whirling are [13], [14]. Rotor whirling in hydropower machines is not uncommon [15] in the forward direction of rotation though backward whirling of a rotor is considered to occur less frequently in practice. The rotor shaft in a vertical hydropower machine is directly connected to the turbine shaft. Thus any forces and dynamics from the water hitting the turbine blades will also affect the rotor.

This article focusses on force or the unbalanced magnetic pull (UMP) predictions under mixed eccentricities condition in a hydropower generator. Mixed eccentricities motion reflects better in practice the motion of the rotor centre in hydropower machines. The predicted estimates are computed by a hybrid method that accounts for computer electromagnetic (EM) simulations together with analytical calculations. The EM simulations part in the method is based on estimating the behaviour of the UMP in the radial and in the tangential directions over a definite but wide whirling frequency range of the rotor centre motion in a purely dynamic eccentricity motion at 10 % value of the mean air-gap length. This wide whirling frequency range encompasses both forward (positive direction) and backward (negative direction) whirling rotations of the rotor. The analytical part of the estimation method rests upon the assumption that the UMP behaviour both in the radial and in the tangential directions thus obtained from the previously mentioned purely dynamic eccentricity motion EM simulations can be scaled linearly for small eccentricities. That said, static eccentricity counterparts up to twice the nominal purely dynamic eccentricity of 10 % have been considered in the mixed eccentricities motion cases analysed to evaluate the robustness of the proposed

method despite that manufacturers tend to limit the amount of overall eccentricity to 10 % of the mean air-gap length [16].

The UMP time series predictions in the Cartesian directions are compared and analysed against the corresponding UMP from the actual EM simulations of the mixed eccentricities motion from Mag-Net [17]. It has been found suitable to use an objective technique such as the feature selective validation (FSV) for the comparison. The FSV method [18]–[22] mimics the response from a group of experts and uses natural language descriptors in a Cooper-Harper scale [23] which has been modified to assess how well two data sets compare with each other.

Many commercial EM analysis software packages cannot handle dynamic eccentricity, and worse a combination of static and dynamic eccentricities. However, the FEM-based EM software package Mag-Net [17] with its ability to set multiple motion components in the EM model has been found suitable for simulating mixed eccentricities condition in the present study. By using information from UMP whirling curves in the suggested hybrid method, this paper accentuates the need for electrical machine designers to consider whirling effects. Two of the authors previously carried out dynamic analyses for a generator considering both the range of forward and backward whirl but where only a purely dynamic eccentricity exists [24], [25]. Thus there is a need to understand the concept of whirling in hydropower generators.

A small-scale synchronous generator [26] which has been specially made available for hydropower research has been used in this study. The EM results and analysis in this paper have been obtained from no-load simulations. Though it can be argued that loading will tend to reduce the magnitude of the UMP, the intention of this article is to find whether the UMP in the mixed eccentricities condition can be predicted to a certain degree of accuracy from purely dynamic eccentricity UMP whirling curves.

For a such complex rotor centre motion as under mixed eccentricities, a couple of days of EM simulations on a fairly recent computer is needed in order to witness important EM parameters such as current and ohmic losses to go to steady state behaviours before the force curves are also stable. Hence the very important goal in this paper of proposing a hybrid method to predict the UMP time histories can save considerable time in the analysis when small eccentricities exist.

II. THE GENERATOR MODEL

A. Physical parameters of the generator unit

A two-dimensional model of the rotor and the stator of the generator was considered sufficient for the modelling on the computer as skewing effect of the rotor is absent. The main parameters of the 185 kW 3-phase salient-pole type alternator that are useful in the simulations are given in Table I. The rotor poles sit outwards on the rotor rim which in turn is fixed on the spider. This is shown in Fig. 1. It is to be noted at this stage that the simulations in this article were carried out using the full two-dimensional model of the generator and not with just the one-pole pitch model as shown in Fig. 1.

All the simulations in this paper are based for the no-load case. This was preferred to the load condition since measurements are easier to do when currents are not flowing in the stator coils. Also, vibrations that appear when the generator is operating on a no-load condition may be masked once the stator terminals start supplying current to a load source.

B. The eddy current problem in a generator

In any electrical machine, there are regions which are conducting and regions which are not conducting in regard to eddy current presence [27]. If we write the Maxwell's Equations with respect to the fixed stator reference frame, then we have [28]
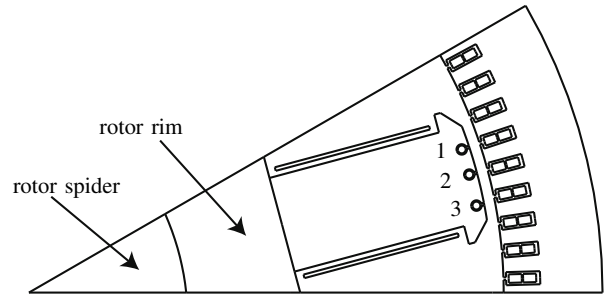

Fig. 1. Fig. shows the cross section of the generator studied for one pole pitch only and when there is no eccentricity. The solid rotor rim sits on the solid spider. The uneven spatial distribution of the three damper bar slots on a pole shoe can also be seen. The two damper bars Bars 1 and 3 on every pole shoe are in an asymmetric configuration around the centre damper slot that holds Bar 2. More explicitly, if a line is drawn from the rotor geometric centre through the centre damper slot, then the angle subtended by the line from the rotor centre though the damper slot for Bar 3 is greater than the corresponding angle for the damper slot with Bar 1 considered instead. In the simulations, the direction of rotation of the rotor is anticlockwise with Bar 1 leading. The damper bar slots are open at the top of the pole shoe

TABLE I
Important dimensions and parameters of the generator

Parameter	Value
Rotor axial length [mm]	305
Rotor spider radius, [mm]	120.1
Rotor rim external radius [mm]	200.1
Rotor external radius[1] [mm]	354.1
Mean air-gap length, [mm]	8.4
Rotor mechanical angular velocity, ω_{ro} [rad/s]	52.36
Number of poles	12
Number of stator slots	108
Slot angle pitch, γ [electrical degrees]	20

[1] *This includes the pole shoe height*

$$\nabla \times \mathbf{H} = \mathbf{J}$$

$$\nabla \times \mathbf{E}_{\text{eddy}} = -\frac{\partial \mathbf{B}}{\partial t}$$

$$\nabla \cdot \mathbf{D} = \rho$$

$$\nabla \cdot \mathbf{B} = 0 \tag{1}$$

where

$$\mathbf{J} = \begin{cases} \mathbf{J}_0 & \text{in } \Omega_{nc}, \\ \sigma \left(\mathbf{E}_{\text{eddy}} + \mathbf{v}_{ro} \times \mathbf{B} \right) & \text{in } \Omega_c. \end{cases} \tag{2}$$

In Equation (2), the region Ω_{nc} refers to the non-conducting domain with boundary Γ_{nc} and Ω_c refers to the eddy current conducting domain with Γ_c as its boundary respectively. A solution to the magnetic field in the whole domain $\Omega_{nc} \cup \Omega_c$ only becomes possible when the coupling that exists at the interface(s) between the separate regions in terms of the continuity of $\mathbf{H} \times \mathbf{n}$ and $\mathbf{B} \cdot \mathbf{n}$ is maintained and the constitutive equations of matter are introduced as well. For a two-dimensional setting, a generator will have a magnetic vector potential A_z and current density J_z. Equations (1) and (2) can then be cast together as

$$-\frac{\partial^2 A_z}{\partial x^2} - \frac{\partial^2 A_z}{\partial y^2} = \mu J_z \tag{3}$$

and

$$-\frac{\partial^2 A_z}{\partial x^2} - \frac{\partial^2 A_z}{\partial y^2} = -\sigma\,\mu\,\frac{\partial A_z}{\partial t} + \sigma\,\mu\,\left(\mathbf{v}_{\mathrm{ro}} \times \left[\frac{\partial A_z}{\partial y} - \frac{\partial A_z}{\partial x}\right]\right) \quad (4)$$

with the boundary condition as $A_z = 0$ on the stator yoke of the generator. A list of common assumptions governing Maxwell's equations as applied to electrical machines is listed in references [29], [30].

C. Parameters used in the simulations

For all the simulations, the EM model was set up with no running up of the rotor. In other words, the speed of the rotor was at its synchronous value right from the start of the simulations and this remains so till the end of the simulations. Moreover, the model makes all current sources to be on at the onset of the simulation. The time step in the transient simulations had a value of 0.1 ms and it took 120 ms of simulation time for a fixed point on the rotor to make one complete revolution.

The rotor geometry consists of a solid spider at the middle, on which the solid rotor rim is fixed. The poles sit outside on the rotor rim and are laminated as is the stator. Eddy currents in the solid spider and in the solid rotor rim have thus been taken into account in the simulations.

As mentioned in Section I, the force predictions rest upon two steps. The first step covers the EM simulations part where purely dynamic eccentricity UMP curves at 10 % of the mean air-gap length (see Table I) were made over a wide whirling frequency range, and different whirling speeds have been considered in the simulations within a range of six times the synchronous velocity (or the rotor mechanical angular velocity) of $\omega_{\mathrm{ro}} = 52.36$ rad/s both in the positive and in the negative whirl direction (see Table II). These simulations have as aim to form the UMP whirling curves as shown in Fig. 2 in Section II-D1. Three rotor revolutions were found sufficient in this part of the EM simulations, and currents and the ohmic losses converge rapidly. The other EM simulations done in this paper dealt with the true modelling of the mixed eccentricities motion. The different motion cases considered for analysis are listed in Table III. Here, six rotor revolutions were required and the information pertaining to the last three revolutions was kept in subsequent analysis.

TABLE II

Whirling speeds range used in the purely dynamic eccentricity simulations

Whirling ratio, ω_{whr}	Whirling speed [deg/s][1]	Whirling speed [rad/s]
−6.0	−18 000	-314.16
1.0[2]	3 000	52.36
6.0	18 000	314.16

[1] *This unit can be conveniently set within MagNet [17]*
[2] *This value represents synchronous whirl and has been included in the table to give an idea of the magnitudes of the whirling speeds used in the simulations*

TABLE III

Mixed eccentricities motion cases studied

Case	Dynamic eccentricity [%][1]	Static eccentricity [%][1]
A	10	5
B	10	20
C	5	10
D	5	20

[1] *The eccentricity value is taken of the mean air-gap length given in Table I*

For the start of every motion case studied in this paper be it for the purely dynamic eccentricity cases or for the mixed eccentricities motion cases as given in Table III, the initial position of the rotor has been set to lie on the positive side of the Cartesian x-axis. For all simulations done, it is to be expected that as the rotor whirls, the flux densities on the rotor vary as well which in turn affect the whirling velocity of the rotor. This additional complexity was not introduced in the model. In particular for the purely dynamic eccentricity EM simulations, for each whirling frequency considered the rotor has been set to whirl with that constant whirling velocity for the whole duration of the simulations. The goal with this simulation type is to find the steady state field solutions corresponding to a particular whirling frequency. Using this principle, Fig. 2 can be made. For the mixed eccentricities motion cases as given in Table III, the motion of the purely dynamic eccentricity for the synchronous case (see Table II) has been superimposed onto a static motion. Synchronous positive whirling with respect to the purely dynamic eccentricity motion counterpart in the mixed eccentricities motion has been selected since the latter is a common case in practice as it is a stable operating condition [25]. Finally it is to be emphasised that for all simulations done in this paper, the rotor centre motion takes prescribed motion trajectories i.e. the coordinates of the geometric centre of the rotor are specified in the EM software package.

It is to be noted that in all the EM simulations, the magnetomotive force of the field windings was constant at 2430 A turns. Also, the damper bars were connected in a circuit as a squirrel cage with interconnections between poles. Moreover, vents and cooling ducts were not modelled in the EM analysis since these geometric features will only require finer mesh densities in the finite element analysis, which can increase the solver time considerably.

D. Theoretical development for force prediction

The procedure for estimating the forces in the Cartesian x and y directions for the case of mixed eccentricities motion can be broken down in two major steps. The first step as outlined next in Section II-D1 describes the estimation of the radial and tangential UMP components from the Cartesian force time histories in MagNet [17]. The second step involves the calculations of the forces in the Cartesian x and y directions for mixed eccentricities motion using the UMP whirling frequency curves given in Fig. 2 on the assumption that the UMP can be scaled linearly with the radial eccentricity for small eccentricities. This part is explained in Section II-D2.

1) Radial and tangential UMP computations

EM simulations were carried out in MagNet [17] for a purely dynamic eccentricity rotor centre motion of 10 % over a wide whirling ratio range of −6.0 to 6.0 (see Table II) with the intent to obtain the distribution of the forces acting on the rotor as a function of the whirling ratio or whirling frequency. MagNet [17] computes the forces in the horizontal and in the vertical directions acting on the rotor through the latter's centre of mass. For the rotor under study that is assumed to be homogeneous and that has a perfectly circular structure, this centre of mass coincides with the geometric centre of the rotor.

It is to be noted that for the purely dynamic eccentricity motion, F_x and F_y have sinusoidal variations with time that are governed by the whirling frequency; For example, if the constant whirling frequency used is the synchronous whirling frequency (see Table II), then the period for one oscillation is 120 ms. This time corresponds to one full revolution of the rotor. Now, the UMP is suitably expressed in the radial direction, F_r, and in the tangential direction, F_t. The UMP components, F_r and F_t, are computed at each time step and after which their mean values are estimated. This process is repeated for other whirling frequencies in the whirling ratio range of interest i.e.

from -6.0 to 6.0. The mean values of F_r and F_t over a time sequence used in the EM simulations thus obtained correspond to the steady state UMP values at that specific whirling frequency.

Afterwards, transfer function fits [31] using the least-squares criterion were made to these force curves of F_r and F_t as a function of the whirling ratio. Transfer functions consisting of the minimum number of coefficients were chosen that do not have poles in the desired domain of whirling ratios, ω_{whr}, i.e. from -6.0 to 6.0. The estimated rational function models are given in order, by Equation (5a) and (5b), and the coefficients A's and B's are provided in Appendix A. Fig. 2 shows the fitted curves for the radial and tangential UMP together with the simulation points.

$$F_{r,\,d}^{UMP}(\omega_{whr,\,d}) = -\frac{A_{0r} + A_{1r} \times \omega_{whr,\,d} + A_{2r} \times \omega_{whr,\,d}^2}{B_{0r} + B_{1r} \times \omega_{whr,\,d} + B_{2r} \times \omega_{whr,\,d}^2} \quad (5a)$$

$$F_{t,\,d}^{UMP}(\omega_{whr,\,d}) =$$
$$-\frac{A_{0t} + A_{1t} \times \omega_{whr,\,d} + A_{2t} \times \omega_{whr,\,d}^2 + A_{3t} \times \omega_{whr,\,d}^3}{B_{0t} + B_{1t} \times \omega_{whr,\,d} + B_{2t} \times \omega_{whr,\,d}^2 + B_{3t} \times \omega_{whr,\,d}^3} \quad (5b)$$
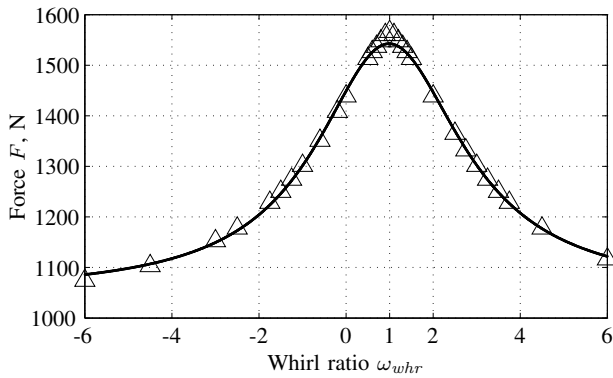
(a) Radial force distribution on the rotor
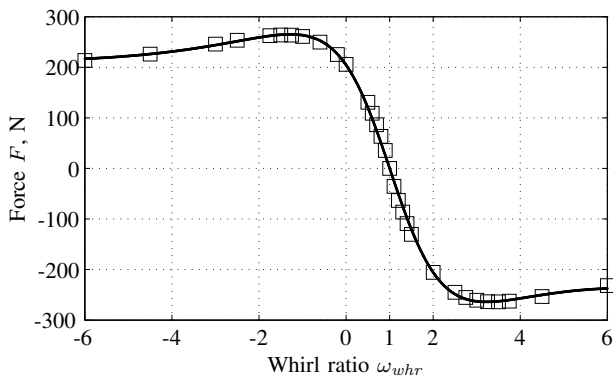
(b) Tangential force distribution on the rotor

Fig. 2. Radial force and tangential force distributions on the rotor with a purely dynamic eccentricity motion of 10 % of the mean air-gap length. The transparent triangles and squares on the graphs depict the whirling frequencies used in the EM simulations. The continuous lines represent the least-squares rational function fits and the fits coefficients are provided in Appendix A. Synchronous whirl occurs at the point when $\omega_{whr,\,d} = 1$

2) Force predictions in mixed eccentricities motion

In this article, the UMP curves in Fig. 2 obtained at 10 % purely dynamic eccentricity are the building bricks on which force estimation for other eccentricity values rests. The schematic used for the derivation of useful quantities is shown in Fig. 3 where $x_s > x_d$ and x_s is in the positive Cartesian x-direction at time $t = 0$.
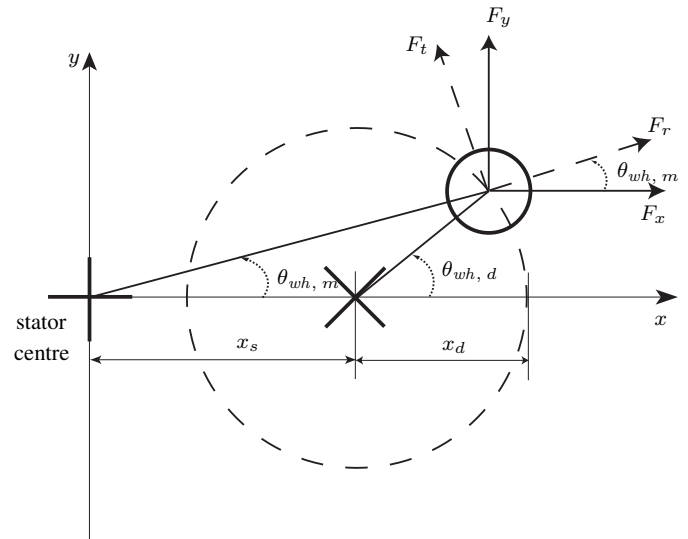

Fig. 3. Schematic of the geometry used to define the location of the forces and the different whirling angles in a mixed eccentricities motion. The true whirling angle $\theta_{wh,\,m}$ in the mixed eccentricities case is different from the whirling angle $\theta_{wh,\,d}$ of the purely dynamic eccentricity case. The axis of rotation of the rotor centre is shown by the symbol x. The geometric centre of the rotor is shown at a time instant t other than zero by the symbol o. All whirling angles are measured anticlockwise i.e. in the positive sense with respect to the direction of the rotation of the rotor

In Fig. 3, the equations of motion of the geometric centre of the rotor can be written in the Cartesian coordinates system as

$$x = x_s + x_d \, \cos(\theta_{wh,\,d}); \quad (6a)$$
$$y = x_d \, \sin(\theta_{wh,\,d}) \quad (6b)$$

where the whirling angle $\theta_{wh,\,d} = \omega_{wh,\,d}\, t$. Equation (6) can now be cast into

$$\tan(\theta_{wh,\,m}) = \frac{y}{x} \quad (7)$$

where the whirling angle $\theta_{wh,\,m}$ is defined in Fig. 3 and is the whirling angle for the mixed or combined eccentricities motion. If we take the derivative of Equation (7) with respect to time, we end up with the following equation:

$$\dot{\theta}_{wh,\,m} = \frac{x \cdot \dot{y} - y \cdot \dot{x}}{x^2 + y^2} \quad (8)$$

The limitation of Equation (8) is obvious in that it cannot handle the case where the denominator becomes zero. This can happen in the case where x_s is equal to x_d (see Fig. 3), in which case the rotor geometric centre will pass through the stator geometric centre at some point in time.

The estimation for the UMP F_x and F_y for the case of mixed eccentricities motion is then as follows: For each time instant used in the EM simulations for the purely dynamic eccentricity motion

(a) Compute the true whirling frequency $\dot{\theta}_{wh,\,m}$ from Equation (8);

(b) Calculate the true whirling ratio as $\omega_{whr} = \frac{\dot{\theta}_{wh,\,m}}{\omega_{ro}}$;

(c) Calculate the radial, F_r, and tangential, F_t, UMP using the above whirling ratio, ω_{whr}, in Equation (5a) and (5b), and according to Fig. 2;

(d) Compute the eccentricity ratio, x_r, which is given by $x_r = \frac{\sqrt{x^2 + y^2}}{x_d}$ with the radial eccentricity in the mixed eccentricities case given by $\sqrt{x^2 + y^2}$;

(e) Scale the UMP computed in part (c) linearly with this eccentricity ratio, x_r to get F_r^{pred} and F_t^{pred};

(f) Finally, estimate the UMP F_x^{pred} and F_y^{pred} for the mixed eccentricities motion case as follows:

$$F_x^{pred} = F_r^{pred} \times \frac{x}{\sqrt{x^2+y^2}} - F_t^{pred} \times \frac{y}{\sqrt{x^2+y^2}}; \quad (9a)$$

$$F_y^{pred} = F_r^{pred} \times \frac{y}{\sqrt{x^2+y^2}} + F_t^{pred} \times \frac{x}{\sqrt{x^2+y^2}} \quad (9b)$$

III. THE FEATURE SELECTIVE VALIDATION METHODS

There are several validation methods available [19]. Their aim is to quantify the similarity of two data sets, making these validation methods an objective tool for test engineers to discuss data on a similar basis. They also offer the possibility of a quantitative assessment of the ranked results to be interpreted as expert opinion [32]. The validation method most widely used today because of its versatility and simplicity in the field of electromagnetic compatibility is the feature selective validation (FSV) method [33], [34], which now incorporated into IEEE standard 1597.1 [22], has the advantage of analysing the two major aspects that are widely considered to be paramount in any validation: The magnitude levels and the shape of the graphs describing the data.

The FSV method is based on the separation of the data to be compared into two groups: The difference in amplitude characterised by the amplitude difference measure (ADM), and the difference between the detailed characteristics of the signal characterised by the feature difference measure (FDM) [33]. The ADM compares the amplitudes and trends in the data sets which represent the slow variation of the shape of the data whereas the FDM compares the rapidly changing features of fast variation in the shape of the data in the data sets [32], [35]. The lower the ADM and FDM, the better is the comparison between two data sets.

The two metrics ADM and FDM perform a point-by-point analysis. By studying the point-by-point data, it is possible to know which areas of the data set have the dominant differences. A subscript "i" is added to consider this point-by-point feature (specifically the ADMi and FDMi). The ADM indicator of the IEEE-FSV method is calculated according to the following equation [20]:

$$ADM(k) = \left| \frac{\left(|Lo_1(k)| - |Lo_2(k)|\right)}{\frac{1}{N}\sum_{j=1}^{N}\left(|Lo_1(j)| + |Lo_2(j)|\right)} + ODMi(k) \cdot e^{ODM(k)} \right| \quad (10)$$

with

$$ODM(k) = \frac{\chi(k)}{\delta} \quad (11)$$

where

$$\chi(k) = \left| \left(|DC_1(k)| - |DC_2(k)| \right) \right|; \quad (12)$$

$$\delta = \left| \frac{1}{N}\sum_{j=1}^{N}\left(|Lo_1(j)| + |Lo_2(j)|\right) \right| \quad (13)$$

DC data is the very low component of the original data, "Lo" is the low-frequency component of the original data, N is the length of the data sets under comparison, and k iterates between 1 to N data points. The offset difference measure (ODM) in Equation (10) represents a contribution to the ADM that is due to the difference between the offsets of the two data sets being compared. The FDM indicator for a particular frequency f of the Fourier Transform of the data in the IEEE-FSV method is calculated according to:

$$FDM(f) = 2\left(|FDM_1(f) + FDM_2(f) + FDM_3(f)| \right) \quad (14)$$

with

$$FDM_1(f) = \frac{|Lo_1'(f)| - |Lo_2'(f)|}{\frac{2}{N}\sum_{i=1}^{N}\left(|Lo_1'(i)| + |Lo_2'(i)|\right)}; \quad (15)$$

$$FDM_2(f) = \frac{|Hi_1'(f)| - |Hi_2'(f)|}{\frac{6}{N}\sum_{i=1}^{N}\left(|Hi_1'(i)| + |Hi_2'(i)|\right)}; \quad (16)$$

$$FDM_3(f) = \frac{|Hi_1''(f)| - |Hi_2''(f)|}{\frac{7.2}{N}\sum_{i=1}^{N}\left(|Hi_1''(i)| + |Hi_2''(i)|\right)} \quad (17)$$

where "Lo" and "Hi" are the low- and high-frequency components of the original data respectively obtained after applying data filtering. Lo′ and Hi′ are the first derivatives of the data of the low and high frequency components respectively, and Hi″ is the second derivative of the high frequency component. The Hi and Lo refers to the Fourier Transform of the data.

After the ADMi and FDMi values have been calculated, it is possible to find a corresponding average value. Such an indicator, XDMtot, is very useful for quickly evaluating the quality of the results with a single number and the lower the value, the better is the agreement between the data sets being compared:

$$XDMtot = \frac{1}{N}\sum_{k=1}^{N}XDMi(k) \quad (18)$$

where XDMtot refers to either the ADMtot or to the FDMtot.

Finally, the IEEE-FSV method provides a tool to make a qualitative interpretation of the results by a coarse probability density function using the point-by-point values for each indicator to form the ADMc and FDMc confidence histograms respectively which are useful for a rapid and comprehensive analysis of the results as presented in Table IV. These histograms are sorted according to qualitative descriptors into Excellent, Very good, Good, Fair, Poor and Very poor to reflect the view of experts. The six-point rating is a modified Cooper-Harper scale that is derived from the original ten-point Cooper-Harper Scale [36] introduced in 1969 to aid pilots assess flying qualities of aircrafts.

TABLE IV
FSV interpretation scale for ADMc and FDMc histograms

FSV quantitative value	FSV qualitative interpretation
Less than 0.1	Excellent
Between 0.1 and 0.2	Very good
Between 0.2 and 0.4	Good
Between 0.4 and 0.8	Fair
Between 0.8 and 1.6	Poor
Greater than 1.6	Very Poor

This efficient and rapid method of analysis is ideal for most signals. However, previous studies have identified some problems when applying the IEEE-FSV [22] to analyse particular signals [35], [37], [38]. In order to overcome these drawbacks and to make a correct validation, a variation of the IEEE-FSV method has been developed [39], [40] and is known as FSV-UPC [41]. The main change from the IEEE-FSV method lies in the correction of the ODM indicator and implementation of soft transitions for DC and "Lo" data set.

The ODM indicator in Equation (11) in its present form is severely affected by smaller offset levels [38], [40]. The reason can be found in the smaller offset in the signals when the value of "δ" in Equation (13) decreases and the ODM grows. This error directly affects to the ADMi indicator. This is an important drawback in all signals that have offset levels close to zero.

The ODM indicator deviations are solved by applying an offset level correction factor (DC_{cor}) to both signals. This change will only affect the values of the ODM indicator, reducing the influence of " δ "

in the ADM indicator [40]. Furthermore, an offset level correction factor (DC_{cor}) is applied to both signals ensuring that there will be no zero crossing; This is to overcome gradient normalisation when the magnitude of the derivatives are taken for FSV calculation, which can give rise to errors in FSV when multiple zero-crossings are included in the original data but the offsetting does not take away the accuracy of the FSV method. The equations used are:

$$DC_{1,2} = Data_1(t) + DC_{cor}; \quad (19)$$

$$DC_{cor} = \max\Big(\max\big(|Data_1(t)|\big),\ \max\big(|Data_2(t)|\big)\Big) \quad (20)$$

Finally, the transitions of the very low frequencies regions are smoothed. In the original FSV (the IEEE-FSV method), the DC data is calculated taking the first five samples from both data in the Fourier domain. However, subsequent studies have shown that it is better to take only the first three samples and then applying a triangular filter to ensure a smooth transition. The application of this simple filter on the d.c. data and "Lo" data reduces significantly the effect caused by the sudden DC transition which is defined in the IEEE-FSV method. The FSV-UPC method has been applied in this paper as it has been found to give better results than the IEEE-FSV method.

IV. RESULTS AND ANALYSIS

A. Estimated forces and their validation

This section has as aim to present the forces obtained from the EM simulations with MagNet [17] for the truly simulated motion mixed eccentricities and those using Equation (9a) (which rests upon the estimation of the forces based on the 10 % purely dynamic eccentricity simulations done earlier in MagNet). In the purely dynamic eccentricity component of the mixed eccentricities motion, synchronous whirl was imposed as this is a common operating point of a hydropower generator. The EM simulations for the mixed eccentricities motion were done for six rotor revolutions and the steady state force time histories after three revolutions have been considered for analysis in this section. The FSV method with its ADMc and FDMc indicators are also used to give a qualitative and quantitative assessment of the similarities and differences in the forces from the two previously-mentioned methods. The objective of the FSV method is to provide measures of how close the UMP predictions from Equation (9a) are with the truly UMP in MagNet [17]. The indicators in the validation process have been computed using the FSV-UPC method from the software in reference [41]. The results shown in this article have been limited to the force in the Cartesian x-direction. It is to be noted however that the force in the other Cartesian direction presented similar characteristics. The different mixed eccentricities motion cases that are considered in this paper are given in Table III.

Moreover, estimates of the spectrum contents for each of the force from the two different methods have been provided as an aid to identify the frequency component(s) that a complex motion as in the case of mixed eccentricities may engender. The spectrum amplitudes have been scaled down by the sampling frequency of the time histories and have no physical meaning. The force estimates using the two methods with their corresponding spectrum estimates together with the ADMc and FDMc indicators for different motion cases are presented in Figs 4 to 7 in order of increasing static eccentricity for each dynamic eccentricity case as tabulated in Table III. In Figs 4 to 7 the Cartesian horizontal force time series obtained with MagNet [17] refer to the actual simulation of the combined eccentricities motion in the software. The predicted UMP force F_x^{pred} is computed according to Equation (9a) together with Fig. 2.
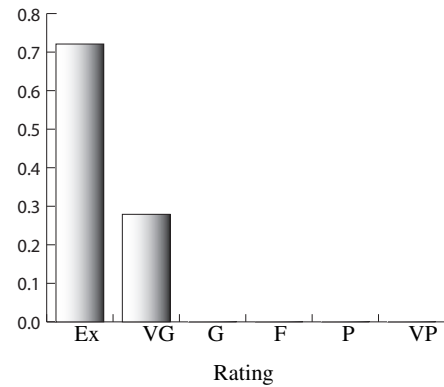
Three main things of interest emerge from Figs 4 to 7: Firstly, the spectral estimates are clean and show only one tonal component apart the d.c. value. This tonal component is explained by the whirling
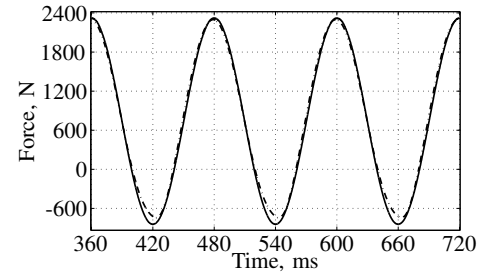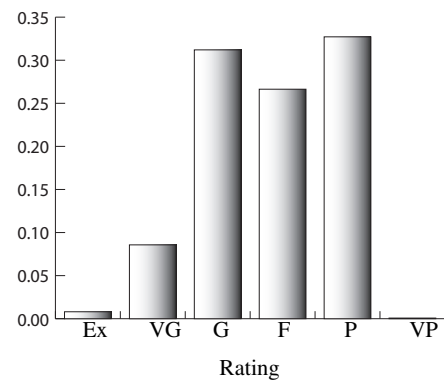

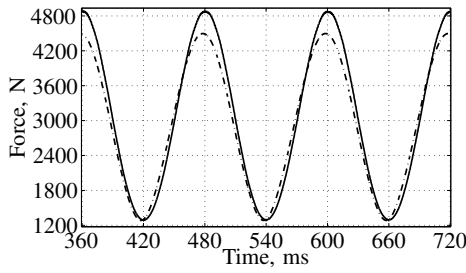(a) Force time histories
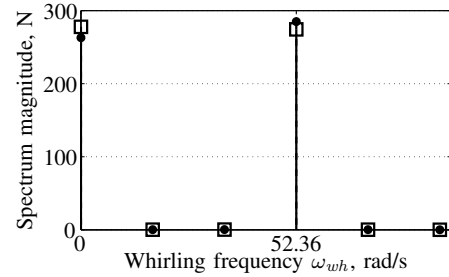
(b) FFT of time histories
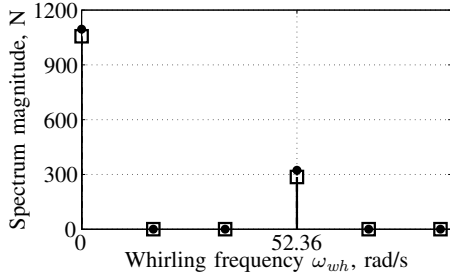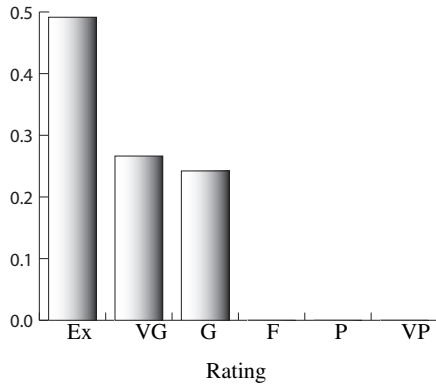

(c) ADMc indicator

(d) FDMc indicator

Fig. 4. Fig. 4a shows the time histories after three revolutions of the Cartesian horizontal forces obtained with MagNet [17] and with Equation (9a) as solid line and dash-dotted line respectively for motion case A in Table III. Fig. 4b presents the spectrum contents of the force time histories of Fig. 4a as stem plots ending in solid circles for MagNet [17] force estimate and in transparent squares for the force estimate in Equation (9a). The amplitudes of the spectrum estimates have been scaled down by the sampling frequency and have no physical relevance. A dynamic whirl ratio of unity corresponds to a dynamic whirling frequency of $\omega_{wh,\,d} = 52.36$ rad/s. Fig. 4c displays the ADMc indicator whereas Fig. 4d displays the FDMc indicator
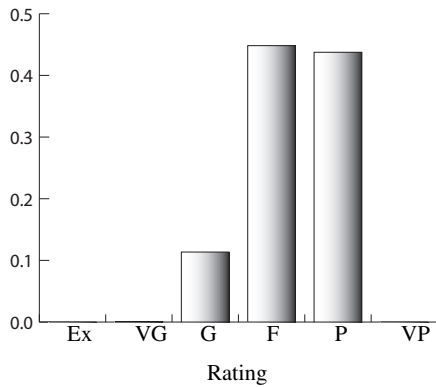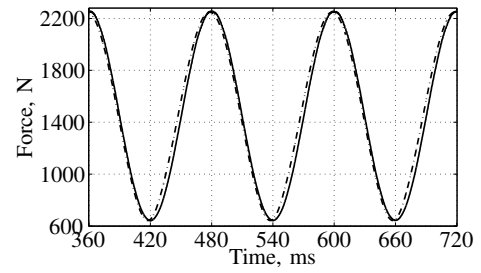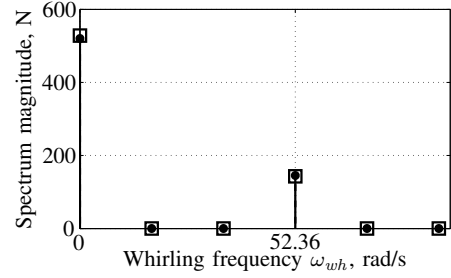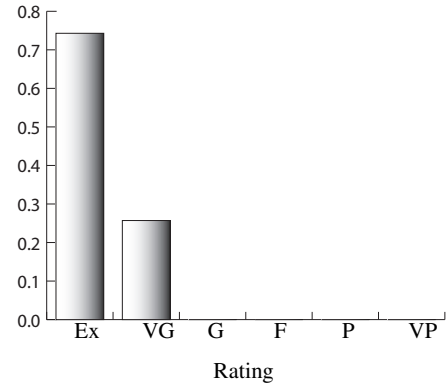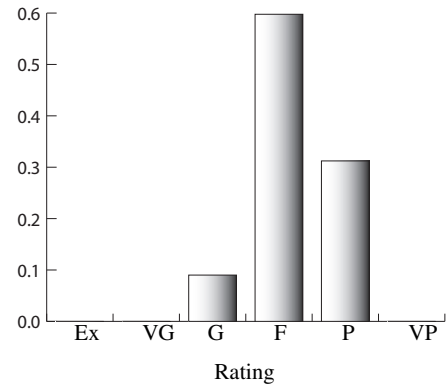
(a) Force time histories

(b) FFT of time histories

(c) ADMc indicator

(d) FDMc indicator

Fig. 5. Fig. 5a shows the time histories after three revolutions of the Cartesian horizontal forces obtained with MagNet [17] and with Equation (9a) as solid line and dash-dotted line respectively for motion case B in Table III. Fig. 5b presents the spectrum contents of the force time histories of Fig. 5a as stem plots ending in solid circles for MagNet [17] force estimate and in transparent squares for the force estimate in Equation (9a). The amplitudes of the spectrum estimates have been scaled down by the sampling frequency and have no physical relevance. A dynamic whirl ratio of unity corresponds to a dynamic whirling frequency of $\omega_{wh,d} = 52.36$ rad/s. Fig. 5c displays the ADMc indicator whereas Fig. 5d displays the FDMc indicator

(a) Force time histories

(b) FFT of time histories

(c) ADMc indicator

(d) FDMc indicator

Fig. 6. Fig. 6a shows the time histories after three revolutions of the Cartesian horizontal forces obtained with MagNet [17] and with Equation (9a) as solid line and dash-dotted line respectively for motion case C in Table III. Fig. 6b presents the spectrum contents of the force time histories of Fig. 6a as stem plots ending in solid circles for MagNet [17] force estimate and in transparent squares for the force estimate in Equation (9a). The amplitudes of the spectrum estimates have been scaled down by the sampling frequency and have no physical relevance. A dynamic whirl ratio of unity corresponds to a dynamic whirling frequency of $\omega_{wh,d} = 52.36$ rad/s. Fig. 6c displays the ADMc indicator whereas Fig. 6d displays the FDMc indicator

frequency of the rotor with respect to the purely dynamic eccentricity motion which is at the synchronous speed of 52.36 rad/s (see Table II). No other tonal component was observed in the spectrum estimates at higher frequencies. Secondly, looking at the coarse probability density functions that the indicators ADMc and FDMc display in Figs 4 to 7, it is seen clearly that a deterioration in the estimated UMP versus the truly simulated UMP appears with increasing static eccentricity and this is expected. With the ADMc and FDMc indicators, Fig. 4 is to be compared with Fig. 5, whereas Fig. 6 is to be compared with Fig. 7 respectively. A small phase difference is noted somehow in the UMP time series of the two methods. This can be perhaps explained by the finite time step that is used in the simulations in MagNet [17]. Thirdly, it is observed from Figs 4 to 7 that with small addition of a static eccentricity value to the dynamic eccentricity value, the steady state UMP predictions from Equation (9a) are in good agreement amplitude-wise with the steady state UMP from MagNet [17]. Although not shown in the paper, only motion case A in Table III had a positive whirling ration $\omega_{whr, m}$ at all time instants and used the UMP whirling curve of Fig. 2a around $\omega_{whr, d} = 1$ where the fit made suffered its largest amplitude error in the UMP F_r. A positive whirling ratio as in motion case A is in accordance with what is to be expected when the static eccentricity has a smaller value than its dynamic counterpart.

V. CONCLUSIONS

This paper aimed at stressing the need for engineers to consider the whirling dependent behaviour of the rotor centre motion in hydropower generators. To this end, it has been shown how an analytical equation (Equation (8)) in combination with Fig. 2 can be used in the prediction of forces in the case of mixed eccentricities motion. This equation together with Equation (6) can in fact be used for any kind of rotor centre motion that can be prescribed in terms of the coordinates of the rotor centre. Though a caveat exists in that the denominator of Equation (8) cannot be zero, this equation forms the method that has been proposed in this paper and promising results have been reported as seen in Figs 4 to 7. Therefore, the suggested hybrid method in Section II-D2 which rests upon the premise that a linear scaling of the UMP levels at small eccentricities is possible is valid.

A now standardised procedure used in computational electromagnetics [42] namely the feature selective validation method has been applied successfully to provide qualitative and quantitative assessment between the truly EM simulations UMP and the predicted UMP at steady state. Instead of providing a single value for the comparison, the ADMc and FDMc indicators express the assessments in terms of slow and fast variations in the data that would be obtained with a team of experts in the field. A modified FSV method namely the FSV-UPC was adopted as it provided better results than the IEEE FSV [22] method.

The modelling of a complex motion such as in the mixed eccentricities case is not a trivial task even in contemporary FEM-based EM software packages. A typical mixed eccentricity simulation in MagNet [17] takes about 73 hours to do six rotor revolutions on a modern quad-core computer operating under Windows 7 according to the simulation parameters of Section II-C. The results in this study have shown that for small enough eccentricities, one can use the method which has been put forward in this paper to arrive at very good estimates of the steady state UMP quickly. The closeness to the UMP in the truly EM simulations rests upon the fits that are made to the UMP whirling curves (Fig. 2). For the mixed eccentricities simulations in this paper, it was found that the whirling ratios used varied between -2.0 to 2.0, indicating that considering a large whirling ratio range from -6.0 to 6.0 as shown in Fig. 2 is sufficient for ordinary cases that may exist in practice. Figs 4 to 7 indicate that the actual UMP
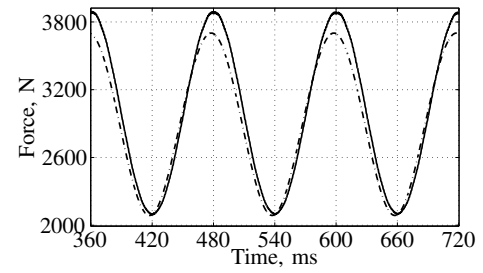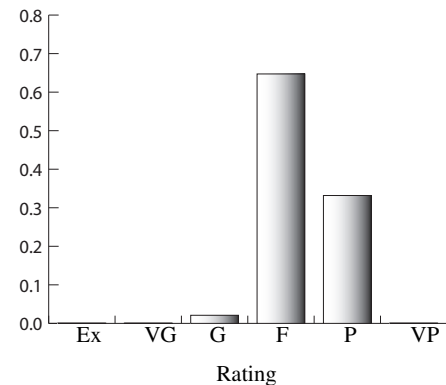

(a) Force time histories
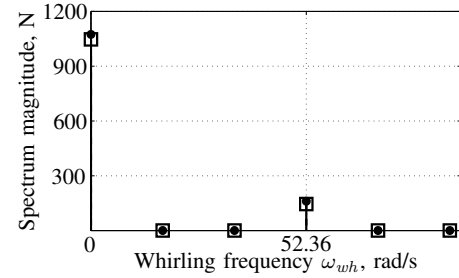
(b) FFT of time histories
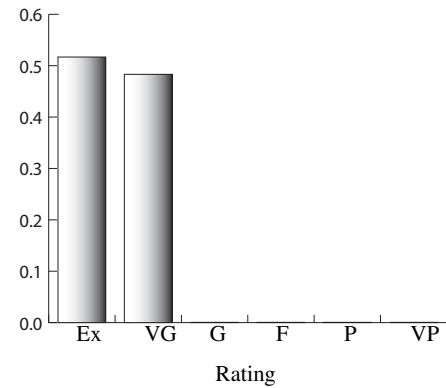
(c) ADMc indicator

(d) FDMc indicator

Fig. 7. Fig. 7a shows the time histories after three revolutions of the Cartesian horizontal forces obtained with MagNet [17] and with Equation (9a) as solid line and dash-dotted line respectively for motion case D in Table III. Fig. 7b presents the spectrum contents of the force time histories of Fig. 7a as stem plots ending in solid circles for MagNet [17] force estimate and in transparent squares for the force estimate in Equation (9a). The amplitudes of the spectrum estimates have been scaled down by the sampling frequency and have no physical relevance. A dynamic whirl ratio of unity corresponds to a dynamic whirling frequency of $\omega_{wh, d} = 52.36$ rad/s. Fig. 7c displays the ADMc indicator whereas Fig. 7d displays the FDMc indicator

computed with MagNet [17] is higher than the predicted UMP with larger static eccentricities. This can be attributed to the fact that the linear scaling assumption as proposed in Section II-D2 starts to fail with higher eccentricities.

The EM analyst will thus have to generate the UMP dependent whirling curves for a sufficiently reasonable range with sufficient whirling points considered and apply the proposed method of Section II-D2 in order to be able to predict the UMP behaviours for different motion types. He has only to ensure that the reference UMP curves for the purely dynamic eccentricity motion that he produces is based on an eccentricity value that is in the linear part of the B-H curve. The rotor centre coordinates for any motion type can be computed on a computer with information regarding the rotor mechanical angular velocity or spin speed, the static eccentricity, the dynamic eccentricity and the whirling velocity for the dynamic eccentricity counterpart, and the time discretisation to be used. Though only results in the Cartesian x-direction are shown in the paper, it has been found that the force predictions in the other Cartesian direction had similar behaviours.

The simulations and results presented in this paper were carried out with a synchronous whirl of the rotor with respect to the purely dynamic eccentricity component in the mixed eccentricity model. This local synchronous whirl has been chosen as it reflects a typical operation point of a hydropower generator. Of course, the suggested method allows for any other desired whirling frequency as well.

The essence of new contribution to the field of EM analysis of hydropower generators from this article is the presentation of the importance of whirling and how it can be used to predict UMP time series. This is of paramount importance as the FSV method has shown some very good agreements when low eccentricities exist. Hours of EM simulation time can be saved by the new suggested hybrid method after UMP whirling dependent curves have been produced as given in Fig. 2.

ACKNOWLEDGMENTS

APPENDIX
Coefficients of the rational UMP components

A.1 Radial UMP component

The coefficients of Equation (5a) to seven decimal places are as follows:

$$A_{0r} = -1\,448.824\,951\,2$$
$$A_{1r} = 392.748\,626\,7$$
$$A_{2r} = -203.668\,151\,9$$
$$B_{0r} = 1$$
$$B_{1r} = -0.377\,557\,5$$
$$B_{2r} = 0.194\,205\,3 \tag{A.1}$$

A.2 Tangential UMP component

The coefficients of Equation (5b) to seven decimal places are given next:

$$A_{0t} = -204.652\,984\,6$$
$$A_{1t} = 218.872\,329\,7$$
$$A_{2t} = -17.781\,187\,1$$
$$A_{3t} = 3.107\,314\,3$$
$$B_{0t} = 1$$
$$B_{1t} = -0.460\,365\,3$$
$$B_{2t} = 0.220\,089\,2$$
$$B_{3t} = -0.006\,302\,5 \tag{A.2}$$

It is to be noted that the constant terms B_{0r} and B_{0t} occurring in the denominators of $F_{r,\,d}^{UMP}$ and $F_{t,\,d}^{UMP}$ respectively (see also Equation (5)) were set to unity in the least-squares fit estimation.

REFERENCES

[1] M. Walker. *Specification and Design of Dynamo-Electric Machinery*. Longmans' Electrical Engineering Series, 1915.

[2] E. Rosenberg. Magnetic pull in electrical machines. *Transactions of the American Institute of Electrical Engineers*, 37(2):1425–1469, 1918.

[3] I. Ozelgin. Analysis of magnetic flux density for airgap eccentricity and bearing faults. *International Journal of Systems Applications, Engineering & Development*, 4(2):162–169, 2008.

[4] D. de Canha, W.A. Cronje, A.S. Meyer, and S.J. Hoffe. Methods for diagnosing static eccentricity in a synchronous 2 pole generator. In *Power Tech, 2007 IEEE Lausanne*, pages 2162–2167, July 2007.

[5] I. Tabatabaei, J. Faiz, H. Lesani, and M.T. Nabavi-Razavi. Modeling and simulation of a salient-pole synchronous generator with dynamic eccentricity using modified winding function theory. *IEEE Transactions on Magnetics*, 40(3):1550–1555, May 2004.

[6] G. Joksimovic, C. Bruzzese, and E. Santini. Static eccentricity detection in synchronous generators by field current and stator voltage signature analysis—part I: Theory. In *Electrical Machines (ICEM), 2010 XIX International Conference, Rome, Italy*, pages 1–6, 6-8 Sept. 2010.

[7] B.A.T. Iamamura, Y. Le Menach, A. Tounzi, N. Sadowski, and E. Guillot. Study of static and dynamic eccentricities of a synchronous generator using 3-D FEM. *IEEE Transactions on Magnetics*, 46(8):3516 –3519, August 2010.

[8] J. Faiz, M. Babaei, J. Nazarzadeh, B.M. Ebrahimi, and S. Amini. Time-stepping finite-element analysis of dynamic eccentricity fault in a three-phase salient pole synchronous generator. *Progress In Electromagnetics Research B*, 20:263–284, 2010.

[9] J. Faiz, B.M. Ebrahimi, M. Valavi, and H.A. Toliyat. Mixed eccentricity fault diagnosis in salient-pole synchronous generator using modified winding function method. *Progress In Electromagnetics Research B*, 11:155–172, 2009.

[10] M. Negrea, P. Jover, and A. Arkkio. Electromagnetic flux-based condition monitoring for electrical machines. In *Fifth IEEE International Symposium on Diagnostics for Electric Machines, Power Electronics and Drives, 2005. SDEMPED*, pages 1–6, 2005.

[11] B.H. Shakibaei. Analysis and simulations of eccentric rotors of rotating machinery in polar space. *World Applied Sciences Journal*, 17(12):1675–1682, 2012.

[12] L. Wu, B. Lu, X. Huang, T.G. Habetler, and R.G. Harley. Improved online condition monitoring using static eccentricity-induced negative sequence current information in induction machines. In *Industrial Electronics Society, IECON 2005*, 31st *Annual Conference of IEEE*, 6–10 November, 2005.

[13] T.P. Holopainen, A. Tenhunen, E. Lantto, and A. Arkkio. Unbalanced magnetic pull induced by arbitrary eccentric motion of cage rotor in transient operation. Part 1: Analytical model. *Electrical Engineering*, 88(1):13–24, April 2005.

[14] T.P. Holopainen, A. Tenhunen, E. Lantto, and A. Arkkio. Unbalanced magnetic pull induced by arbitrary eccentric motion of cage rotor in transient operation. Part 2: Verification and numerical parameter estimation. *Electrical Engineering*, 88(1):25–34, March 2005.

[15] N.L.P. Lundström and J-O. Aidanpää. Whirling frequencies and amplitudes due to deviations of generator shape. *International Journal of Non-Linear Mechanics*, 43(9):933–940, November 2008.

[16] H. Torkaman and E. Afjei. Magnetostatic field analysis regarding the effects of dynamic eccentricity in switched reluctance motor. *Progress In Electromagnetics Research M*, 8:163–180, 2009.

[17] MagNet, Infolytica Corporation, Montréal, Québec, Canada, 2011, Version 7.1.3.

[18] B. Archambeault, S. Connor, and A.P. Duffy. Comparing FSV and human responses to data comparisons. In *International Symposium on Electromagnetic Compatibility, 2005. EMC, Chicago, USA*, volume 1, pages 284–289, August 2005.

[19] A.L. Drozd. Selected methods for validating computational electromagnetic modeling techniques. In *International Symposium on Electromagnetic Compatibility, EMC 2005*, volume 1, pages 301–306, August 2005.

[20] R. Jauregui and F. Silva. Numerical validation methods (editor: Jan Awrejcewicz). In *Numerical Analysis—Theory and Application*. InTech, September 2011.

[21] V. Rajamani, C.F. Bunting, A. Orlandi, and A. Duffy. Introduction to feature selective validation (FSV). In *Antennas and Propagation Society International Symposium 2006, IEEE, 2006, Albuquerque, USA*, pages 601–604, 9–14 July 2006.

[22] IEEE Electromagnetic Compatibility Society. IEEE standard for validation of computational electromagnetics computer modeling and simulations—IEEE std 1597.1$^{\text{TM}}$, 2008.

[23] V. J. Gawron. *Human Performance Measures Handbook*. CRC Press, July 2000.

[24] Y. Calleecharan and J-O. Aidanpää. Dynamics of a hydropower generator subjected to unbalanced magnetic pull. *Proceedings of the Institution of Mechanical Engineers, Part C: Journal of Mechanical Engineering Science*, 225(9):2076–2088, 2011.

[25] Y. Calleecharan and J-O. Aidanpää. Stability analysis of an hydropower generator subjected to unbalanced magnetic pull. *IET Sci. Meas. Technol.*, 5(6):231–243, November 2011.

[26] Division for Electricity, The Ångström Laboratory, Uppsala Universitet, Sweden.

[27] O. Biro. Computational Electromagnetics (CEM) Conference 2011—Review of eddy current analysis. [online]. http://tv.theiet.org/technology/electronics/10890.cfm.

[28] D. Marcsa and M. Kuczmann. Finite element analysis of single-phase induction motors. COMSOL Conference, Budapest, Hungary November 24, 2008, pp. 1-6.

[29] M.V.K. Chari and P. Silvester. Analysis of turboalternator magnetic fields by finite elements. *IEEE Transactions on Power Apparatus and Systems*, PAS-90(2):454–464, March 1971.

[30] John R. Brauer. *Magnetic Actuators and Sensors*. Wiley-IEEE Press, 1$^{\text{st}}$ edition, February 2006.

[31] DATAPLOT. National Institute of Standards and Technology, Technology Administration, U.S. Department of Commerce. Version 5/02/06.

[32] D. Coleby and A. Duffy. Analysis of techniques to compare complex data sets. *COMPEL: The International Journal for Computation and Mathematics in Electrical Engineering*, 21, Iss. 4:540–553, 2002.

[33] A. Duffy, A. Martin, O Antonio, G. Antonini, T. Benson, and M. Woolfson. Feature selective validation (fsv) for validation of computational electromagnetics (CEM). Part i—the FSV method. *IEEE transactions on electromagnetic compatibility*, 48(3):449–459, 2006.

[34] A. Orlandi, A. Duffy, B. Archambeault, G. Antonini, D. Coleby, and S. Connor. Feature selective validation (fsv) for validation of computational electromagnetics (CEM). Part ii—assessment of FSV performance. *IEEE transactions on electromagnetic compatibility*, 48(3):460–467, 2006.

[35] J. Knockaert, J. Peuteman, J. Catrysse, and R. Belmans. Modifying the feature selective validation method to validate noisy data sets. *IET Sci. Meas. Technol.*, 2(4):244–257, 2008.

[36] NASA. Flying qualities, stability and control, and performance evaluations, [Online]. http://history.nasa.gov/SP-3300/ch4.htm.

[37] R. Jauregui, P. Riu, and F. Silva. Transient FDTD simulation validation. *IEEE Proc. International Symposium on Electromagnetic Compatibility, EMC 2010*, pages 257–262, 2010.

[38] P. Riu, R. Jauregui, F. Silva, and M. Fernandez. Transient electromagnetic field computation in automotive environments using FDTD. *IEEE Proc. International Symposium on Electromagnetic Compatibility, EMC 2007, Honolulu, Hawaii*, pages 1–4, July 9–13, 2007.

[39] R. Jauregui, J. Rojas-Mora, and F. Silva. Study of transient phenomena with feature selective validation method. *Progress In Electromagnetics Research*, 7(3):286–290, 2011.

[40] R. Jauregui, F. Silva, A. Orlandi, H. Sasse, and A. Duffy. Factors influencing the successful validation of transient phenomenon modelling. In *Asia-Pacific electromagnetic compatibility symposium and technical exhibition, Beijig, China*, pages 2–5, 2010.

[41] GCEM Validation Tool (GVT), Grup de Compatibilitat Electromagnètica (GCEM), DEE Universitat Politècnica de Catalunya, Barcelona, Spain, Version 3.0.3, November 2012, [Online]. http://www.upc.edu/web/gcem/.

[42] A. Duffy, A. Drozd, B. Archambeault, and D. Coleby. Measuring similarity for validation of computational electromagnetic modelling. In *International Symposium on Electromagnetic Compatibility, EMC 2004*, volume 2, pages 697–702, 9–13 August, 2004.

BIOGRAPHIES

Yogeshwarsing Calleecharan received the B.Eng. degree in Mechanical Engineering from the University of Mauritius, Mauritius, in 2000, the M.Sc. degree in Mechanical Engineering from Blekinge Tekniska Högskola, Sweden, in 2003, and the Ph.D. degree in Solid Mechanics from Luleå Tekniska Universitet, Sweden, in 2013. Since 2014 he is a lecturer with the Mechanical and Production Engineering Department, University of Mauritius, Mauritius. His research interests include electromechanics, vibrations and signal analysis.

Ricardo Jauregui received the B.Sc. degree in Electrical Engineering from Los Andes University, Venezuela, in 2001, the M.Sc. degree in Mobile communication from Desuto University, Bilbao, Spain, in 2003, and the Ph.D. degree from Polytechnic University of Catalonia (UPC), Barcelona, Spain, in 2010. He is currently Program Manager at Roche Diagnostics, Barcelona, Spain. His research interests include the use of different simulation and validation techniques to analyse and solve signal processing issues. In the last years, he has been working on exploring the effect of the transient in frequency and the time domain for complex structures.

Jan-Olov Aidanpää received the M.S. degree in Mechanical Engineering from Luleå Tekniska Universitet (LTU), Sweden, in 1987, and the Ph.D. degree in Solid Mechanics from LTU in 1995. Since 2013 he is working as Chair Professor in Computer Aided Design at Luleå Tekniska Universitet, Sweden. His research interest is within non-linear rotor dynamics where he develops measuring techniques and models of hydro and wind power systems.